

Surface States and Arcless Angles in Twisted Weyl Semimetals

Ganpathy Murthy¹, H.A. Fertig², and Efrat Shimshoni³

¹ *Department of Physics and Astronomy, University of Kentucky, Lexington, KY 40506-0055*

² *Department of Physics, Indiana University, Bloomington, IN 47405 and*

³ *Department of Physics, Bar-Ilan University, Ramat-Gan 52900, Israel*

(Dated: September 23, 2019)

Fermi arc states are features of Weyl semimetal (WSM) surfaces which are robust due to the topological character of the bulk band structure. We demonstrate that Fermi arcs may undergo profound restructurings when surfaces of different systems with a well-defined twist angle are tunnel-coupled. The twisted WSM interface supports a moiré pattern which may be approximated as a periodic system with large real-space unit cell. States bound to the interface emerge, with interesting consequences for the magneto-oscillations expected when a magnetic field is applied perpendicular to the system surfaces. As the twist angle passes through special “arcless angles”, for which open Fermi arc states are absent at the interface, Fermi loops of states confined to the interface may break off, without connecting to bulk states of the WSM. We argue that such states have interesting resonance signatures in the optical conductivity of the system in a magnetic field perpendicular to the interface.

Introduction – Weyl semimetals (WSM’s) are three-dimensional materials which host electronic structures with unusual, robust topological properties. Their bulk band structures contain an even number of “Weyl points,” locations where the constant energy surfaces shrink to a point, which act as sources or sinks of Berry’s flux through two-dimensional surfaces surrounding them^{1,2}. Their presence in such materials leads to a number of remarkable phenomena, including non-conservation of currents associated with individual Weyl nodes in co-linear electric and magnetic fields, and an associated negative longitudinal magnetoresistance^{1,3}. WSM’s can arise in spin-orbit coupled systems with either broken inversion symmetry⁴ or time-reversal symmetry^{5–8}. For the latter anomalous Hall effects^{9,10} are expected, as well as non-local transport properties^{11–13}.

Intimately connected with many of these phenomena is the presence of “Fermi arc” states^{5,14} in finite size WSM’s. For a semi-infinite WSM, there is a two-dimensional (surface) Brillouin zone (BZ) which generically hosts bound surface states. At zero energy (defined as the energy of the Weyl points), Fermi arcs are one or more curves in the surface k -space that connect the projections of the Weyl points onto the surface BZ. For any k that a Fermi arc passes through, there is a state carrying surface current perpendicular to the arc itself. At the arc endpoints, the penetration depth of the surface state diverges, allowing for exchange between surface and bulk currents. Indeed, in a slab placed in a magnetic field perpendicular to the surfaces, current may flow in opposite directions along Fermi arcs on each surface, connected by chiral states through the bulk, to form closed loops¹⁵. These periodic orbits are expected to generate magneto-oscillations in measurable properties of a slab of WSM^{16,17}. Notably, because the orbits involve a bulk component, the characteristic frequencies depend on the slab thickness.

Given the remarkable nature of surface states in WSM’s, it is interesting to explore how their properties might be modified and/or controlled. This is the subject of our study. Specifically, we consider the fate of Fermi arc states when surfaces from two separate WSM’s are twisted with respect to one another, and then tunnel-coupled. Tunnel-coupling of dis-

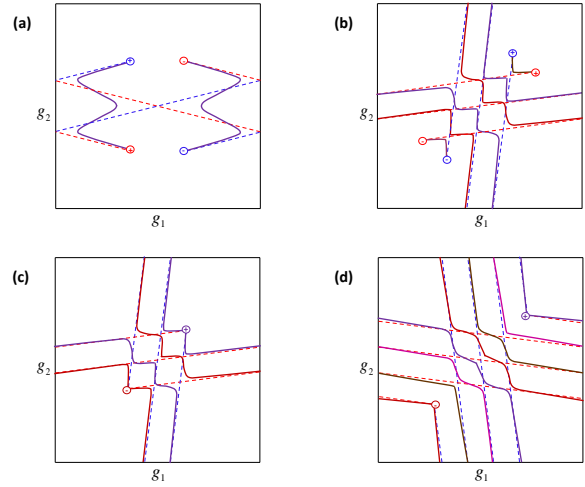


FIG. 1: Reconstructed Fermi arcs patterns in the moiré Brillouin zone for various values of the twist angle θ : (a) $\theta < \pi/4$; (b) an arbitrary $\pi/4 < \theta < \pi/2$; (c) the arcless angle θ_1 , where two closed loops are generated; (d) the arcless angle θ_{-2} , yielding two distinct pairs of closed loops (of which only one pair connects to the Weyl nodes). Dashed blue (red) lines represent the original arcs on the top (bottom) WSM slab.

tinct Weyl fermion systems aligned with one another along high-symmetry directions are known to admit Fermi arc states which can connect Weyl nodes of different subsystems^{18,19}. In this work we consider general rotation angles, and find that the possibilities for Fermi arc reconstruction are considerably richer. This physics emerges from the lattice misalignment at the interface, resulting in a moiré pattern that can be approximated by a two-dimensional lattice with a large real-space unit cell. Analogous physics is known to be important in twisted graphene bilayers and other two-dimensional van der Waals bonded systems^{20,21}. In the graphene case, the prediction of extremely flat bands in the effective moiré Brillouin zone^{22,23} has been indirectly verified by the demonstration of interaction-induced correlated states^{24,25} that one might expect of such systems.

Tunneling between states on the two WSM surfaces can occur directly between states of the same crystal momentum (“direct tunneling”), or between states whose wavevectors differ by linear combinations of the reciprocal lattice vectors in each layer (“umklapp tunneling”). When the layers are separated by a distance greater than the lattice constant of the underlying crystals, the umklapp processes are dominated by the shortest scattering wavevectors; retaining just the two smallest of these (along with the direct tunneling term) results in an effective surface superlattice defined by the two scattering wavevectors, along with a corresponding moiré Brillouin zone. We find that, generically, the coupled Fermi arcs within a moiré Brillouin zone will oscillate in direction (as shown in Fig. 1a), and typically connect Weyl nodes of the two different slabs^{18,19}. For some ranges of angles, one finds that Fermi arcs reconstruct to form open arcs connecting the Weyl nodes, coexisting with arcs that close upon themselves. For special “arcless angles”, the interface hosts *only* closed Fermi loops. For relatively weak coupling, some of these loops include points at the surface projections of the Weyl points, while for stronger coupling the Weyl points may couple directly to one another, so that all the Fermi loops at the interface are completely disconnected from the Weyl points. A summary of these different possibilities is illustrated in Fig. 1.

The existence of closed Fermi loops at the arcless angles is particularly interesting. For sufficiently clean systems this means the interface hosts two types of conducting channels. Type (i) channels go through the Weyl point projections, and have significant overlap with the bulk at the Weyl points. Type (ii) channels never intersect the Weyl point projections, and thus do not leak into the bulk of either system. In the presence of a perpendicular magnetic field, currents associated with type (ii) channels should flow along the arc. Although they present open orbits in real space – and are thus not expected to lead to oscillations in the density of states – they involve periodic motion due to the meandering of the orbits through the moiré Brillouin zone, with periods inversely proportional to the magnetic field. This suggests the interface will present resonances in its optical conductivity $\sigma(\omega)$ that reflect the orbit periods, in analogy with the behavior of “warped” open orbits at the Fermi surface of quasi-one-dimensional materials²⁶. Type (i) orbits similarly should present oscillations in $\sigma(\omega)$; however, because they are *closed* in real space they are additionally expected to result in density of states magneto-oscillations which can be detected in thermodynamic quantities at zero frequency¹⁵. In the perturbative regime of tunnel-coupling, for type (i) orbits the resonance frequency in $\sigma(\omega)$ is expected to jump as the twist angle crosses an arcless angle. For type (ii) orbits, the frequency itself evolves continuously as a function of twist angle, but the amplitude of $\sigma(\omega)$ should jump as arcless angles are crossed.

We now turn to a more detailed discussion of our results, as well as the analysis that leads to them.

Model Hamiltonian and Surface States – Our starting point is a simple two-band model⁶ (with broken time-reversal symmetry) of a WSM hosting two Weyl nodes, supporting a single Fermi arc on any surface for which the projections of the Weyl points do not overlap in the surface Brillouin zone. The under-

lying crystal is cubic (with lattice constant as our length unit), and the bulk Hamiltonian as a function of crystal momentum takes the form

$$H_0(\mathbf{k}, k_z) = 2 \sum_{\mu=x,y,z} f_\mu \sigma_\mu. \quad (1)$$

In this expression, \mathbf{k} is a two-dimensional momentum, σ_μ are Pauli matrices, and $f_x = t(2 + \cos k_0 - \cos k_x - \cos k_y - \cos k_z) \equiv t(1 - \cos k_z) + \tilde{f}_x$, $f_y = t \sin k_y$, and $f_z = t' \sin k_z$. The bulk Weyl points are $(\pm k_0, 0, 0)$. To simplify our notation, we hereon set $t = 1$. The existence and form of surface states may be found by going to the continuum limit in one direction, which we take here to be \hat{z} . Expanding $H_0(\mathbf{k}, k_z)$ to second order in k_z , we can look for evanescent solutions by taking $k_z \rightarrow i\lambda$. Within this procedure^{27–29}, four values of λ satisfying $H_0(\mathbf{k}, i\lambda)\Phi = E\Phi$ may be found, two of which produce wave functions that vanish as $z \rightarrow \infty$. One must then choose the value of E such that the eigenvector Φ is the same for both these values of λ , so that a linear combination may be formed satisfying vanishing boundary conditions at $z = 0$. (Details are provided in the SM, Sec. I.) Three points resulting from this analysis are particularly relevant to what follows: (i) For the model defined by Eq. 1, the procedure described above can only be carried through for $|k_x| < k_0$. Thus the surface states are present on an open arc in the surface momentum space. (ii) Eigenstates of H_0 of this form satisfy $E = f_y(k_y) \approx k_y$, so that the states have a velocity along the \hat{y} direction. (iii) The eigenvectors that result from the analysis are spin-polarized along the σ_y direction. For this simple model we can also obtain surface states directly within the tight-binding model (SM, Section II), yielding results consistent with the continuum approximation. The lattice analysis has strengths complementary to the continuum approach, in particular allowing the possibility of making the tunnel-coupling nonperturbative, which we explore in detail in the SM, Sections III and IV.

Twisted WSM’s and Tunnel Coupled Fermi Arcs – Consider a pair of semi-infinite WSM’s, one exposing a top surface and the other a bottom surface, each with a Fermi arc oriented at angles $\pm\theta$ with respect to the \hat{x} -axis. For our model, the Fermi arc state dispersions near zero energy can be written in the form $E_{T,B}(\mathbf{k}) \approx \mathbf{v}_{T,B} \cdot \mathbf{k}$, with $\mathbf{v}_T \cdot \mathbf{v}_B = -v_0^2 \cos 2\theta$. In a long-wavelength model in which the tunneling amplitude is uniform across the surfaces, the two-dimensional crystal momentum will be conserved. Projecting into the Fermi arc states of the two surfaces, the coupled Hamiltonian may be modeled as

$$H_c = \begin{pmatrix} \mathbf{v}_T \cdot \mathbf{k} & w_d \\ w_d & \mathbf{v}_B \cdot \mathbf{k} \end{pmatrix}, \quad (2)$$

where we have assumed w_d is real. In principle, after projection onto the surface states w_d is a function of \mathbf{k} , and should vanish at the positions of the arc end points, for which one of the inverse length scales λ in the surface state construction vanishes, indicating the Fermi arc state crosses over into a bulk state. However, w is most important near $k = 0$ where the Fermi arcs cross, and is non-vanishing at that location. Diagonalizing H_c yields energies $E_\pm = -v_0 \sin \theta k_x \pm$

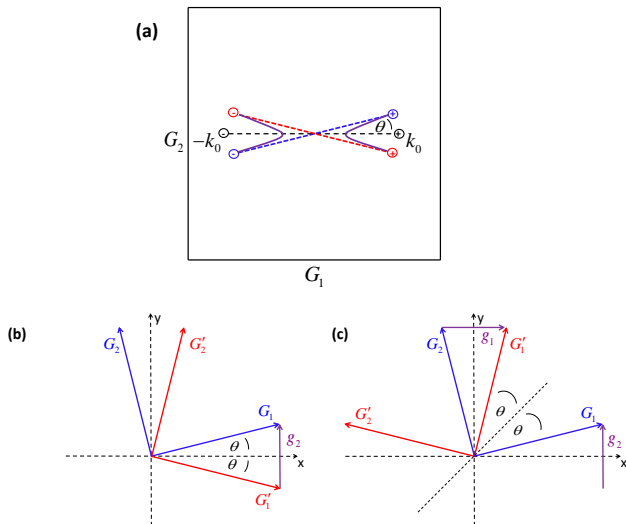


FIG. 2: (a) Zero energy contours (solid purple curves) resulting from the reconstruction of Fermi arcs (dashed lines) on the coupled surfaces of twisted WSM's. (b) Primitive lattice wavevectors of the top and bottom surfaces for a small twist angle ($\theta < \pi/4$). (c) Primitive lattice vectors of the top and bottom surfaces for a twist angle $\pi/4 < \theta < \pi/2$; the wavevectors $\mathbf{g}_1, \mathbf{g}_2$ define the moiré Brillouin zone.

$[v_0^2 \cos^2 \theta k_y^2 + w_d^2]^{1/2}$, whose zero energy contours are illustrated in Fig. 2(a). Note that these reconstructed Fermi arcs now connect Weyl nodes on opposite sides of $z = 0$.

In reality, the two surfaces each have a square lattice structure, and this makes the physics notably richer. Primitive lattice vectors for the top (bottom) surface may be written as $\mathbf{G}_1^{(t)}$ and $\mathbf{G}_2^{(t)}$ as illustrated in Fig. 2(b) for a small twist angle. A simple model incorporating this²² assumes that the tunneling amplitude between atoms in different systems depends only on the total distance between them; summing over the two-dimensional direct lattice vectors then leads to tunneling processes in which the in-plane wavevector scatters by a difference in reciprocal lattice vectors, $\mathbf{g}_{ij} \equiv n_i \mathbf{G}_i - n'_j \mathbf{G}'_j$, with $i, j = 1, 2$ and n_i, n'_j integers. Provided the states are further apart than the underlying lattice constants of the bulk materials, tunneling amplitudes will drop rapidly with increasing $|n_i|, |n'_j|$. The largest amplitudes for such umklapp tunneling processes occur when one of these integers vanishes and the other is ± 1 . These processes may be regarded as renormalizations of the direct tunneling process. Qualitatively new behavior emerges when $|n_i| = |n'_j| = 1$, and translation of the Fermi arcs by \mathbf{g}_{ij} causes them to overlap at new locations in momentum.

The Hamiltonian for states projected onto the Fermi arcs in this case takes the form

$$H_c = \begin{pmatrix} \mathbf{v}_T \cdot (\mathbf{k} + \mathbf{g}_{ij}) & w_u \\ w_u & \mathbf{v}_B \cdot \mathbf{k} \end{pmatrix}, \quad (3)$$

where w_u is a tunneling amplitude associated with the umklapp process defined by \mathbf{g}_{ij} . Within the assumptions discussed

above we expect $|w_u| \ll |w_d|$; however, for values of \mathbf{k} such that $\mathbf{v}_T \cdot (\mathbf{k} + \mathbf{g}_{ij}) \approx \mathbf{v}_B \cdot \mathbf{k}$ its effect cannot be neglected. By retaining just the vectors \mathbf{g}_{ij} that generate such degeneracies, one can describe the system in terms of an effective superlattice, which may be viewed as an approximation to the moiré pattern²² expected to appear at the interface between the two WSM's. Using this paradigm, we next turn to some of the interesting reconstructions of the Fermi arcs that result from this physics.

Results – We begin by considering the situation for small θ . In this case there is a single pair of collinear scattering vectors, $\pm \mathbf{g}_1$ where $|\mathbf{g}_1| = 2 \sin \theta |\mathbf{G}_1|$ (see Fig. 2(b)), which are relevant to the Fermi arc restructuring. In this case the system may be regarded as a one-dimensional superlattice, and an example of the Fermi arc behavior is illustrated in Fig. 1(a). We assume the “bare” Fermi arcs to be short compared to the surface Brillouin zone sizes of the individual layers; nevertheless, for small enough θ the reconstructed Fermi arcs oscillate back and forth repeatedly, ultimately connecting a Weyl node of the lower system to one for the upper system. As θ increases the number of oscillations decreases, and ultimately the reconstructed Fermi arcs will turn back once around $\mathbf{k} = 0$ through a direct process to connect nodes in opposite layers.

An interesting consequence of this behavior is its effect on magneto-oscillations expected for WSM slabs¹⁵. For two rotated slabs tunnel-coupled in this way, in a magnetic field B perpendicular to the interface, semiclassical orbits will pass through the reconstructed arcs. While the total arc length and the effective Lorentz forces along most sections of the arcs are rather similar to their values for uncoupled arcs, at the crossing points the Lorentz force becomes $\sim Bv_0 \sin \theta$, leading to a lengthening of the total orbit period at small θ , both because of the slow velocity at an orbital turning point, and because of the proliferation of the number of such turns as $\theta \rightarrow 0$. This should lead to an anomalous increase of the magneto-oscillation period at small twist angles, which is eliminated as the twist angle increases, both continuously as the velocity around the turning points increases, and in steps as the “switchbacks” in the interface orbits are eliminated.

Fig. 1(b) illustrates the situation for a twist angle satisfying $2\theta \sim \pi/2$. The relevant scattering wavevectors in this case are $\pm \mathbf{g}_1$ and $\pm \mathbf{g}_2$, where $\mathbf{g}_1 \equiv \mathbf{G}'_1 - \mathbf{G}_2$, $\mathbf{g}_2 \equiv \mathbf{G}'_2 + \mathbf{G}_1$ [see Fig. 2(c)]. These wavevectors form an effective small Brillouin zone $[\mathbf{g}_1, \mathbf{g}_2]$ that defines the wavevector space for the periodic approximation to the moiré pattern at the twist interface. Because of the two-dimensional character of this Brillouin zone, the pattern of avoided crossings breaks up the Fermi arcs into a pair of short Fermi arcs connecting Weyl points in the two different systems, and one or more longer closed loops wrapping around the torus defined by the moiré Brillouin zone. For specific twist angles, the Weyl nodes overlap perfectly, eliminating the Fermi arcs, but leave behind the closed orbits (Fig 1c and 1d). These “arcless angles” satisfy the equation

$$\tan\left(\frac{\pi}{2} - 2\theta_n\right) = \frac{k_0}{k_0 + 4\pi n}, \quad (4)$$

with n an integer. The situation at such angles is unique, in

that the twisted WSM supports $2|n|$ closed loops of surface states. In the perturbative regime, two of these closed loops go through the Weyl point projections (type (i) loops), while $2(|n| - 1)$ of them are composed of purely interface states (type (ii) loops). The number of such closed loops changes with twist angle, becoming arbitrarily large as $2\theta \rightarrow \pi/2$. Note that at the arcless angles, even the two type (i) Fermi loops at the interface that nominally overlap with the Weyl point projections may actually detach from them at strong enough tunnel-coupling, as we demonstrate in Sec. IV of the SM for a specific geometry. In such cases, *all* surface states form closed loops disconnected from the Weyl point projections. For small inter-surface coupling, it seems likely that the type (i) Fermi loops will contain the Weyl point projections.

Finally we note that for relative twist angles $2\theta \sim \pi$ and $2\theta \sim 3\pi/2$, one expects to encounter restructured arc states with forms qualitatively similar to those for small twist angles and for $2\theta \sim \pi/2$, respectively.

Discussion – The closed Fermi loops that form at twist interfaces for relative angle $2\theta \sim \pi/2$ of type (ii), and of both types at the arcless angles, represent one of the more surprising phenomena occurring in the twisted WSM system. A direct probe of electrons in these states involves their semiclassical dynamics in a magnetic field \mathbf{B} perpendicular to the interface. The relevant equations of motion are

$$\begin{aligned} \frac{d\mathbf{k}}{dt} &= -e\mathbf{E} - \frac{e}{c}\mathbf{v}_\alpha \times \mathbf{B}, \\ \mathbf{v}_\alpha(\mathbf{k}) &= \nabla \varepsilon_\alpha(\mathbf{k}). \end{aligned} \quad (5)$$

In these equations, \mathbf{k} is contained in the moiré Brillouin zone, and α labels different disconnected parts of the reconstructed Fermi arcs.³⁰ The energy function $\varepsilon_\alpha(\mathbf{k})$ corresponding to the closed Fermi arc is given approximately, over most of its length, by the Fermi arc energies for the uncoupled systems, appropriately translated into the moiré Brillouin zone. For trajectories near zero energy at $\mathbf{E} = 0$, and for $0 \leq \theta \leq \pi/4$ one should set $\varepsilon_\alpha = E_-$ (with E_- as defined below Eq. (2)) near degeneracy points.

First we focus on type (ii) loops. The orbits of Eqs. (5) are closed orbits in the moiré Brillouin zone, but open in real space. Magneto-oscillations in the electronic density of states are not expected; however, the periodicity of the k space orbit should generate excitations of finite frequency, detectable by resonances in the optical conductivity $\sigma(\omega)$ ²⁶.

As θ (assumed near $\frac{\pi}{2}$) decreases the period of the type (ii) closed orbits in \mathbf{k} decreases, and the frequency of the resonance in $\sigma(\omega)$ increases smoothly as a function of θ . However, every time an arcless angle is crossed, the number of type (ii) closed loops changes by two, which should lead to a jump in the resonance *amplitude* in $\sigma(\omega)$. (These statements are strictly correct for weak tunnel-coupling, for which all closed loops are expected to have the same period for a given \mathbf{B} .) Interestingly, because the orbits generating these resonances oscillate both within the plane and perpendicular to them, they should be detectable via absorption of electromagnetic waves polarized either parallel or perpendicular to the interface³¹.

For generic angles, the type (i) interface orbits that connect to the bulk Weyl points should admit more general magneto-

oscillations¹⁵, with period dependent on length of the Fermi arcs at the interface, as well as those at the more remote surfaces, which will also produce resonances in $\sigma(\omega)$. As the Fermi arcs abruptly change length when θ passes through an arcless angle, we expect jumps in the resonance frequency in $\sigma(\omega)$ due to type (i) orbits.

Finally, we briefly comment on the situation for WSM's where the Weyl nodes appear due to broken inversion symmetry, rather than broken time-reversal symmetry. A model bulk Hamiltonian of such a system, with four bands,³² has the form³³

$$H(k) = \lambda \sum_{\mu=x,y,z} \sigma_\mu \sin k_\mu + \tau_y \sigma_y M_k, \quad (6)$$

where $M_k = m + 2 - \cos k_x - \cos k_z$, τ_μ are Pauli matrices acting in an orbital space and σ_μ acts in a spin space. For this model we do not find situations in which closed Fermi loops form at the interface which are disconnected from the Weyl nodes. Nevertheless, three-dimensional closed orbits should still form in a magnetic field, which pass through the interface states. At small twist angles some of these loops will acquire an anomalously long period in the same way as was found above in the system with broken time-reversal symmetry. We again expect this to lead to magneto-oscillations of suppressed frequency.

In real materials, surfaces can have significantly larger numbers of Fermi arcs, which may connect amongst one another along arcs of non-vanishing curvature. At small twist angles we expect such systems will also host low frequency magneto-oscillations. It is interesting to speculate that some such systems might also host closed Fermi loops as found in the two-band model, as well the elimination of open Fermi arcs connecting some of the bulk Weyl nodes. We leave these questions for future research.

Acknowledgements – This work was supported by the US-Israel Binational Science Foundation (Grant No. 2016130: GM, HAF, ES; Grant No. 2018726: HAF, ES), by the NSF (Grant Nos. DMR-1506263, DMR-1506460, DMR-1914451), and by the Israel Science Foundation (ISF) Grant No. 231/14 (ES). The authors acknowledge the hospitality and support of the Aspen Center for Physics (Grant No. PHY-1607611), where part of this work was done. GM is grateful to the Gordon and Betty Moore Foundation for sabbatical support at MIT, and the Lady Davis Foundation for sabbatical support at the Technion, while these ideas were being formed.

I. SUPPLEMENTAL MATERIAL: SURFACE STATES AND ARCLESS ANGLES IN TWISTED WEYL SEMIMETALS

Our Supplemental Material is organized as follows. We start our discussion with the continuum model in Section IA, which has the advantage of being easy to generalize to the case of tunnel-coupled surfaces of Weyl semi-metals twisted with respect to each other at arbitrary angle. The disadvantage is that one can only incorporate tunnel coupling between the surfaces perturbatively. In Section IB we then develop a lattice formulation for the case of a single semi-infinite slab. We proceed further in Section IC by considering the case of two slabs of identical Weyl semi-metal twisted with respect to each other by $\frac{\pi}{2}$ and tunnel-coupled to one another. The advantage of the lattice formulation is that for twist angles that are multiples of $\pi/2$, it allows a treatment that is nonperturbative in the tunnel-coupling. Finally, in Section ID we modify the Hamiltonian of Eq. (7) to obtain curved Fermi arcs, and show by a lattice calculation that when the tunnel-coupling is sufficiently strong, the Fermi arcs can detach from the projections of the Weyl points, and form closed loops in the surface BZ.

A. Fermi arc states for a single semi-infinite slab: Continuum approach

We start with our tight-binding Hamiltonian of Eq. (1) in the main text, with t set equal to unity from the beginning (and $t' > 0$):

$$H = 2 \sum_{\mu} f_{\mu} \sigma_{\mu}, \quad (7)$$

where $f_x = 2 + \cos(k_0) - \cos(k_x) - \cos(k_y) - \cos(k_z) \equiv 1 - \cos(k_z) + \tilde{f}_x$, $f_y = \sin(k_y)$, and $f_z = t' \sin(k_z)$. (A special case of this model, $t' = 1$, was considered in Ref. 18.) We then employ a small k_z expansion, yielding a continuum approximation in the z direction (where the coordinate z is measured in units of the lattice constant $a = 1$). The functions f_x, f_z now become

$$\begin{aligned} f_x &= \frac{1}{2} k_z^2 + \tilde{f}_x, & \tilde{f}_x &= 1 + \cos(k_0) - \cos(k_x) - \cos(k_y), \\ f_z &= t' k_z. \end{aligned} \quad (8)$$

In a real-space representation of the z direction, the Hamiltonian density acquires the form

$$H(k_x, k_y, z) = -2it' \sigma_z \frac{\partial}{\partial z} + \left(2\tilde{f}_x - \frac{\partial^2}{\partial z^2} \right) \sigma_x + 2f_y \sigma_y. \quad (9)$$

Considering a semi-infinite slab where $z \geq 0$, we then search for eigenvectors $\Phi(z)$ of H (with eigenvalues $E(k_x, k_y)$) which obey vanishing boundary conditions on the surface $z = 0$ and decay in the bulk $z \rightarrow \infty$.

From Eq. (9) it is apparent that $\Phi(z)$ are linear combinations of eigenvectors of the form

$$\Phi_{\lambda}(z) = \Phi_0 e^{-\lambda z}, \quad (10)$$

where $\Re\{\lambda\} > 0$ and Φ_0 is a (z -independent) two-component spinor. Substituting Φ_{λ} in $H\Phi_{\lambda} = E\Phi_{\lambda}$, we obtain a quadratic equation for λ as a function of E, k_x, k_y with the solutions

$$\lambda_{\pm}^2 = 2 \left[\tilde{f}_x + (t')^2 \right] \pm \sqrt{4 \left[\tilde{f}_x + (t')^2 \right]^2 + E^2 - 4 \left[\tilde{f}_x^2 + f_y^2 \right]}. \quad (11)$$

The corresponding eigenvectors are of the form Eq. (10) with

$$\Phi_0^{(\pm)} \equiv \begin{pmatrix} u_{\pm} \\ v_{\pm} \end{pmatrix} = \begin{pmatrix} 2\tilde{f}_x - 2if_y - \lambda_{\pm}^2 \\ E - 2it'\lambda_{\pm} \end{pmatrix}. \quad (12)$$

The resulting eigenstates $\Phi(z) = a_+ \Phi_{\lambda_+}(z) + a_- \Phi_{\lambda_-}(z)$ obey the boundary condition $\Phi(0) = 0$ provided the coefficients a_{\pm} satisfy

$$M \begin{pmatrix} a_+ \\ a_- \end{pmatrix} = 0 \quad \text{with} \quad M = \begin{pmatrix} 2\tilde{f}_x - 2if_y - \lambda_+^2 & 2\tilde{f}_x - 2if_y - \lambda_-^2 \\ E - 2it'\lambda_+ & E - 2it'\lambda_- \end{pmatrix}, \quad (13)$$

which has a solution provided $\det M = 0$. Assuming $\lambda_+ \neq \lambda_-$, this yields the equation

$$-E(\lambda_+ + \lambda_-) + 4it'(\tilde{f}_x - if_y) + 2it'\lambda_+\lambda_- = 0. \quad (14)$$

Assuming that λ_+, λ_- are real, they must obey simultaneously

$$-E(\lambda_+ + \lambda_-) + 4t'f_y = 0 \quad \text{and} \quad 2\tilde{f}_x = -\lambda_+\lambda_- . \quad (15)$$

We next impose the requirement $\lambda_+, \lambda_- > 0$, which implies that the second conditions in Eq. (15) can be satisfied only provided $\tilde{f}_x < 0$. Additionally, for the special case $E = 0$ the first condition yields $f_y = 0$. Recalling the definition of \tilde{f}_x, f_y [Eq. (8)], we conclude that a consistent solution for the surface states exists along the segment $k_y = 0, |k_x| < k_0$. Notably, this is precisely the Fermi arc connecting the two Weyl nodes $(\pm k_0, 0)$. For arbitrary E , we combine Eqs. (11) and (15) to get

$$\begin{aligned} E &= 2f_y , \\ \lambda_{\pm} &= t' \pm \sqrt{(t')^2 + 2\tilde{f}_x} . \end{aligned} \quad (16)$$

Interestingly, when substituted in Eq. (12) to obtain the eigenvectors, we find

$$\begin{pmatrix} u_+ \\ v_+ \end{pmatrix} = \begin{pmatrix} u_- \\ v_- \end{pmatrix} = \frac{1}{\sqrt{2}} \begin{pmatrix} 1 \\ i \end{pmatrix} ; \quad (17)$$

i.e., the surface states are spin-polarized along the σ_y direction, as stated in the main text.

B. Fermi arc states for a single semi-infinite slab: Lattice calculation

In this section we consider the lattice Hamiltonian Eq. (7), and transform to real space in the z -direction, with the lattice sites in this direction labeled by n . The momenta k_x, k_y will be left as parameters. Defining the lattice Fourier transform by

$$c_n(k_x, k_y) = \frac{1}{\sqrt{N_z}} \sum_{k_z} e^{ik_z na} c(k_x, k_y, k_z), \quad (18)$$

$$c(k_x, k_y, k_z) = \frac{1}{\sqrt{N_z}} \sum_n e^{-ik_z na} c_n(k_x, k_y), \quad (19)$$

where the lattice spacing is $a \equiv 1$ and we have suppressed the spin index in the fermion destruction operators $c(k_x, k_y, k_z), c_n(k_x, k_y)$. After a bit of algebra we obtain

$$H(k_x, k_y) = \sum_n \left(-c_{n+1}^\dagger (\sigma_x - it'\sigma_z) c_n - c_n^\dagger (\sigma_x + it'\sigma_z) c_{n+1} + 2c_n^\dagger ((1 + \tilde{f}_x)\sigma_x + f_y\sigma_y) c_n \right). \quad (20)$$

In the above we have suppressed the k_x, k_y arguments in all fermion operators for notational simplicity. For further analysis, it is convenient to rotate the σ -matrices by $\frac{\pi}{2}$ around the x -axis, which has the virtue of making the Hamiltonian purely real. In this basis, the Hamiltonian is

$$H(k_x, k_y) = \sum_n \left(-c_{n+1}^\dagger (\sigma_x + it'\sigma_y) c_n - c_n^\dagger (\sigma_x - it'\sigma_y) c_{n+1} + 2c_n^\dagger ((1 + \tilde{f}_x)\sigma_x + f_y\sigma_z) c_n \right). \quad (21)$$

Since the Hamiltonian is real, the wavefunction can also be chosen real. This will play an important role in the counting argument that shows that the conditions to have a surface state can be met.

To consider a semi-infinite slab, we simply restrict the sum over n to either non-negative or non-positive integers. For specificity, let us consider the bottom surface of a semi-infinite slab, with $n = 0, 1, 2, \dots$. We want solutions that decay into the bulk, so we make the eigenstate ansatz

$$|E, k_x, k_y\rangle = \sum_{n=0}^{\infty} \sum_{s=\uparrow, \downarrow} u^n \Phi_{0s} |n, s\rangle, \quad (22)$$

where $|u| < 1$ for the state to be normalizable. Demanding $H|E, k_x, k_y\rangle = E|E, k_x, k_y\rangle$ leads to the matrix condition on Φ_{0s} , for $n > 0$,

$$\left(u^2 (\sigma_x - it'\sigma_y) + u (E - 2(1 + \tilde{f}_x)\sigma_x - 2\sin(k_y)\sigma_z) + \sigma_x + it'\sigma_y \right) \Phi_0 \equiv M\Phi_0 = 0. \quad (23)$$

In explicit terms, the matrix M is

$$M = \begin{pmatrix} u(E - 2f_y) & 1 + u^2 - 2(1 + \tilde{f}_x) + t'(1 - u^2) \\ 1 + u^2 - 2u(1 + \tilde{f}_x) - t'(1 - u^2) & u(E + 2f_y) \end{pmatrix}. \quad (24)$$

Since the matrix M has a zero eigenvector, its determinant should vanish. This gives a quartic equation for u , which, by changing to the variable

$$\xi = u + \frac{1}{u} \quad (25)$$

can be recast as a quadratic equation,

$$\xi^2(1 - t'^2) - 4\xi(1 + \tilde{f}_x) - (E^2 - 4(1 + \tilde{f}_x)^2 - 4f_y^2 - 4t'^2) = 0. \quad (26)$$

Clearly, we can solve this quadratic and then the auxiliary quadratic $u^2 - u\xi + 1 = 0$ to obtain four values of u . The structure of this auxiliary quadratic shows that the values of u occur in pairs whose product is unity. Thus, either both roots are real, with one being less than unity and the other greater, or they are unimodular and complex conjugates of each other. In the latter case the wavefunctions will not be normalizable, and thus there will be no surface modes.

It is interesting to consider the relation of our approach to that of Ref. 18, which is restricted to $t' = 1$. Clearly, $t' = 1$ is singular in the sense that the quadratic equation Eq. (26) becomes a linear one. This means one of the roots has been pushed off to infinity. Solving the auxiliary quadratic, we see that there are only two physically acceptable roots for u in this case, with only one of them being less than unity in magnitude. Ref. 18 presents many elegant results in this simplified model, but one might worry that the results of the fine-tuned $t' = 1$ model may not be generic. Our analysis demonstrates that in fact they are.

Going back to our problem, let us assume that we have obtained two real values of u , say u_1, u_2 such that $|u_1| < 1$, $|u_2| < 1$. The next step is to find the eigenvectors corresponding to these values of u_i by solving $M(u_i)\Phi_0 = 0$. The final step is to find a linear combination of these solutions

$$\Phi(n) = \alpha_1 u_1^n \Phi_0^1 + \alpha_2 u_2^n \Phi_0^2 \quad (27)$$

that satisfies the boundary condition on the surface, which can be written as

$$\Phi(n = -1) = 0. \quad (28)$$

Since the u_i as well as the wavefunctions are real, so are α_i . The normalization is immaterial for satisfying Eq. (28), which means we can set $\alpha_1 = 1$. Thus, for a given k_x, k_y , we have one real free parameter α_2 , and another real free parameter E . With these two parameters we can indeed satisfy the two conditions represented by Eq. (28). This means a solution exists as long as we can find two real $u(b)_i$, with $|u_i^{(b)}| < 1$. [Note that the superscript (b) denotes the bottom surface.]

Given a u which solves the characteristic equation, we can find the eigenvector corresponding to it by solving Eq. (23). For future reference, the un-normalized spinor can be expressed in two equivalent ways,

$$\begin{aligned} \Phi_0(u, E, k_x, k_y) &= \begin{pmatrix} 1 \\ -\frac{u(E-2f_y)}{u^2(1+t')-2uF_x+1-t'} \end{pmatrix}, \\ \text{or} \\ \Phi_0(u, E, k_x, k_y) &= \begin{pmatrix} -\frac{u(E+2f_y)}{u^2(1-t')-2uF_x+1+t'} \\ 1 \end{pmatrix}. \end{aligned}$$

The solutions turn out to be particularly simple if one assumes $0 < t' = \sin \phi < 1$, and $k_0 < \phi$. For the bottom surface of a semi-infinite slab, the energy is

$$E^{(b)}(k_x, k_y) = 2f_y = 2 \sin k_y. \quad (29)$$

(Note this same result was obtained previously¹⁸ for the specific case $t' = 1$.) Defining $F_x = 1 + \tilde{f}_x = \cos k_0 + \frac{1}{2}(\sin^2 \frac{k_x}{2} + \sin^2 \frac{k_y}{2})$, we find that the two u_i we want are solutions to the vanishing of the lower left entry of the matrix M . Thus

$$1 + u^2 - 2F_x u - t'(1 - u^2) = u^2(1 + \sin \phi) - 2F_x u + (1 - \sin \phi) = 0,$$

yielding the solutions

$$u_{\pm}^{(b)} = \frac{F_x \pm \sqrt{F_x^2 - \cos^2 \phi}}{1 + \sin \phi}. \quad (30)$$

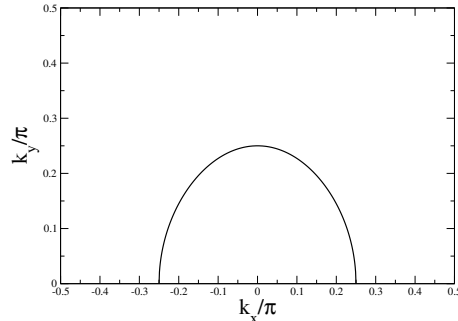


FIG. 3: The region of the surface BZ where Fermi arcs with $E > 0$ on the bottom surface of a semi-infinite slab are allowed in our model. The parameters we have chosen for this plot are $k_0 = \frac{\pi}{4}$, and $t' = 0.8$. There is an identical region for $k_y < 0$ which corresponds to arcs with $E < 0$, again for the bottom surface of a semi-infinite slab, which is not shown.

The Fermi arcs persist within a region of the surface BZ where $F_x < 1$, or equivalently

$$\cos k_x + \cos k_y > 1 + \cos k_0 \quad (31)$$

The region is illustrated in Fig. (3) for $k_0 = \frac{\pi}{4}$. In our simple model the spinors for the bottom surface are always

$$\Phi_i^{(b)} = \begin{pmatrix} 1 \\ 0 \end{pmatrix}, \quad (32)$$

The eigenstates are spin-polarized along the σ_z direction. Recalling the rotation of the Pauli matrices implemented in the beginning of this analysis, this corresponds to polarization along the σ_y direction in the original model Eq. (1).

Now consider the top surface of a semi-infinite slab. In the lattice Hamiltonian the values of n now lie in the range $n = 0, -1, -2, -3, \dots, -\infty$. Instead of the ansatz we made for the bottom surface, Eq. (22), we now make the ansatz

$$|E, k_x, k_y\rangle = \sum_{n=0}^{\infty} \sum_{s=\uparrow, \downarrow} u^{-n} \Phi_{0s} |n, s\rangle. \quad (33)$$

Since n now goes to large negative values we see that we again want values of the two u_i which satisfy $|u_i| < 1$.

The condition for the bulk to satisfy the eigenvalue equation remains the same as Eq. (23), and the four roots of the characteristic equation remain the same. Since, in our model, we have shown that each root occurs with its reciprocal, we simply choose, in the appropriate region (Eq. (31)) the two values of u to be

$$u_i^{(t)} = u_i^{(b)}. \quad (34)$$

For the bottom surface the energy is

$$E^{(t)}(k_x, k_y) = -2f_y = -2 \sin k_y, \quad (35)$$

and the spinor is

$$\Phi^{(t)} = \begin{pmatrix} 0 \\ 1 \end{pmatrix}. \quad (36)$$

At $E = 0$ the Fermi arcs join the projections of the Weyl points onto the surface BZ. The Fermi arc state on the bottom surface has a (group) velocity in the positive y -direction while that on the top surface has a group velocity in the negative y -direction.

We finally comment on the comparison with the continuum approximation described in Sec. I. Within the lattice approach, the eigenstates are parametrized by the multiplicative factor u which denotes a decay of the amplitude within a single lattice constant along the z direction. The continuum solutions Eq. (10) for $z = a = 1$ implies that, in the appropriate limit, one should recover $u = e^{-\lambda}$. In particular, the continuum approximation is valid for $\lambda_{\pm} \ll 1$; from the expression Eq. (16), this is obeyed

for $t' \ll 1$. For simplicity, we further consider a range of k_x where $\tilde{f}_x \ll t' \ll 1$ (so that λ_{\pm} are real). We then recall Eq. (30) for $u_{\pm}^{(b)}$ (with $t' = \sin \phi$ and $\tilde{f}_x = F_x - 1$), and expand $-\ln\{u_{\pm}^{(b)}\}$ to leading order in t', \tilde{f}_x , to find

$$-\ln\{u_{\pm}^{(b)}\} = -\ln\left\{F_x \pm \sqrt{F_x^2 - 1 + (t')^2}\right\} + \ln\{1 + t'\} \approx t' - \tilde{f}_x \mp \sqrt{2\tilde{f}_x + (t')^2} \approx \lambda_{\mp}. \quad (37)$$

Noting that, additionally, the solutions for the energy E and eigenvectors are found to be identical, the continuum limit is indeed recovered in the appropriate limit.

C. Two slabs rotated by $\frac{\pi}{2}$

The key premise of the main text is that when the top surface of one slab of WSM is tunnel-coupled to the bottom surface of another WSM, the Fermi arcs on the two surfaces will hybridize and reconstruct. Generically, since at arbitrary angles of rotation of one surface with respect to the other, there is no true periodicity, and thus no surface BZ, this problem cannot be handled by strictly lattice methods. However, one simple case that can be handled by lattice methods is when two slabs of the same WSM (assumed to have a square lattice in the xy -plane) are rotated with respect to each other by $\frac{\pi}{2}$ and tunnel-coupled. In the following we will assume that the tunnel-coupling between the two surfaces in the z -direction is identical in form to the coupling in the bulk, but may differ in magnitude. We will use c_n , $n = 0, 1, 2, \dots, \infty$ for the operators of the top slab, and d_n , $n = 0, -1, -2, \dots, -\infty$ for the operators of the bottom slab, suppressing the spin and k_x, k_y labels. Bearing in mind that we are rotating the top slab by $\frac{\pi}{2}$ the total Hamiltonian is

$$\begin{aligned} H = & \sum_{n=0}^{-\infty} \left(d_n^\dagger (2 \sin k_y \sigma_z + 2\sigma_x (2 + \cos k_0 - \cos k_x - \cos k_y)) d_n - d_n^\dagger (\sigma_x - it' \sigma_y) d_{n-1} - d_{n-1}^\dagger (\sigma_x + it' \sigma_y) d_n \right) \\ & + \sum_{n=0}^{\infty} \left(c_n^\dagger (-2 \sin k_x \sigma_z + 2\sigma_x (2 + \cos k_0 - \cos k_x - \cos k_y)) c_n - c_{n+1}^\dagger (\sigma_x - it' \sigma_y) c_n - c_n^\dagger (\sigma_x + it' \sigma_y) c_{n+1} \right) \\ & - \kappa d_0^\dagger (\sigma_x + it' \sigma_y) c_0 - \kappa c_0^\dagger (\sigma_x - it' \sigma_y) d_0. \end{aligned} \quad (38)$$

Here κ parameterizes the strength of the tunnel-coupling between the two surfaces. Note the appearance of $-2 \sin k_x$ as the coefficient of σ_z in the site-diagonal term in the Hamiltonian for the top slab. This is because the slab has been rotated by $\frac{\pi}{2}$, leading to $k_x \rightarrow k_y$, $k_y \rightarrow -k_x$. To reduce notational complexity in what follows, we introduce the following definitions.

$$\begin{aligned} f_y^{(t)}(k_x, k_y) &= -\sin k_x, \\ f_y^{(b)}(k_x, k_y) &= \sin k_y, \\ F_x^{(t)} = F_x^{(b)} &\equiv F_x = 2 + \cos k_0 - \cos k_x - \cos k_y, \\ g^{(t)}(u) &= -\frac{u(E - f_y^{(t)})}{u^2(1+t') - 2uF_x + 1 - t'}, \\ g^{(b)}(u) &= -\frac{u(E - f_y^{(b)})}{u^2(1-t') - 2uF_x + 1 + t'}. \end{aligned} \quad (39)$$

For a given E, k_x, k_y let us call the two appropriate roots in the top slab $u_i^{(t)}$, and the two in the bottom slab $u_i^{(b)}$. Generically these will not be the same because $f_y^{(t)}$ and $f_y^{(b)}$ differ. Further defining

$$g_i^{(t)} \equiv g^{(t)}(u_i^{(t)}), \quad g_i^{(b)} \equiv g^{(b)}(u_i^{(b)}), \quad (40)$$

we write the wavefunctions in the top and bottom slabs as

$$\Phi^{(t)}(n) = \alpha_1 (u_1^{(t)})^n \begin{pmatrix} 1 \\ g_1^{(t)} \end{pmatrix} + \alpha_2 (u_2^{(t)})^n \begin{pmatrix} 1 \\ g_2^{(t)} \end{pmatrix}, \quad (41)$$

$$\Phi^{(b)}(n) = \beta_1 (u_1^{(b)})^{-n} \begin{pmatrix} g_1^{(b)} \\ 1 \end{pmatrix} + \beta_2 (u_2^{(b)})^{-n} \begin{pmatrix} g_2^{(b)} \\ 1 \end{pmatrix}. \quad (42)$$

The boundary conditions at the interface can be compactly written as

$$\Phi^{(t)}(n = -1) = \kappa \Phi^{(b)}(0), \quad \Phi^{(b)}(n = +1) = \kappa \Phi^{(t)}(0) \quad (43)$$

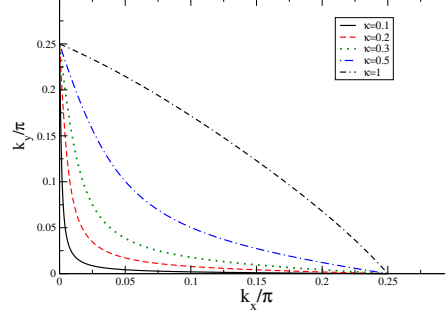


FIG. 4: Reconstructed Fermi arcs for two semi-infinite slabs of identical Weyl semimetals rotated by $\frac{\pi}{2}$ with respect to each other and the free surfaces tunnel-coupled with a strength κ . The parameters we have chosen for this figure are $k_0 = \frac{\pi}{4}$ and $t' = \sin \frac{\pi}{3}$. Only the first quadrant is shown. There is an identical reconstructed Fermi arc in the third quadrant as well. At zero tunnel-coupling the Fermi arcs are un-reconstructed. The Fermi arc belonging to the top slab will be the vertical line $k_x = 0$, $-k_0 < k_y < k_0$, while the Fermi arc belonging to the bottom slab will be the horizontal line $-k_0 < k_x < k_0$, $k_y = 0$. The projections of the Weyl points with positive monopole number are at $(0, k_0)$ (top slab) and $(k_0, 0)$ (bottom slab). As κ increases, the surface states hybridize, and the Fermi arcs reconstruct to reconnect the projections of the + monopoles of the two slabs together and the - monopoles together.

In explicit form, these four equations can be written as

$$\begin{pmatrix} (u_1^{(t)})^{-1} & (u_2^{(t)})^{-1} & -\kappa g_1^{(b)} & -\kappa g_2^{(b)} \\ g_1^{(t)} (u_1^{(t)})^{-1} & g_2^{(t)} (u_2^{(t)})^{-1} & -\kappa & -\kappa \\ \kappa & \kappa & -g_1^{(b)} (u_1^{(b)})^{-1} & -g_2^{(b)} (u_2^{(b)})^{-1} \\ \kappa g_1^{(t)} & \kappa g_2^{(t)} & -(u_1^{(b)})^{-1} & -(u_2^{(b)})^{-1} \end{pmatrix} \begin{pmatrix} \alpha_1 \\ \alpha_2 \\ \beta_1 \\ \beta_2 \end{pmatrix} \equiv M \begin{pmatrix} \alpha_1 \\ \alpha_2 \\ \beta_1 \\ \beta_2 \end{pmatrix} = 0 \quad (44)$$

Now suppose we want to find the reconstructed Fermi arc at the interface for a given value of E . For a solution to exist the determinant of the matrix M must vanish. The only free variables left in M once E is fixed are k_x, k_y , and $\det(M) = 0$ puts one condition on them. This is the implicit equation for the reconstructed Fermi arc. In contrast to the results for the semi-infinite slabs, the reconstructed Fermi arcs for $\kappa \neq 0$ do depend on the value of t' .

In Fig. (4) we show the reconstructed Fermi arc for $E = 0$ for different values of the inter-slab coupling κ . Only the first quadrant of the surface BZ is shown, with a similar reconstruction occurring in the third quadrant.

D. Curved Fermi arcs and detachment from Weyl points

In the main manuscript we noted that at the arcless angles, when the projections of the Weyl points of positive chirality coincide in the surface Brillouin zone (and likewise for the negative chirality Weyl points), the Fermi arcs may form closed loops which are detached from the Weyl points. To demonstrate this requires a nonperturbative calculation in the coupling between the two surfaces. Analogous behavior has been demonstrated for $t' = 1$ ¹⁸, but the special properties of that parameter choice (discussed above) leave open the question of whether such behavior is generic. To address this, we present in this section an analogous calculation demonstrating that Fermi loops can indeed detach from the projections of the Weyl points for sufficiently strong tunnel-coupling, without fine-tuning of parameters.

We modify our model slightly to produce curved Fermi arcs, by changing the functional form of f_y to

$$f_y(k_x, k_y; \lambda) = \sin k_y + \lambda(\cos k_x - \cos k_0). \quad (45)$$

It is easy to see that the bulk Weyl points remain unchanged, regardless of the value of λ . All the manipulations of Section I B go through as before. From Eq. (29), for the bottom surface of a semi-infinite slab, the Fermi arc at $E = 0$ is given by

$$E = 2f_y(k_x, k_y; \lambda) = 0. \quad (46)$$

Let us choose the top semi-infinite slab as above with $\lambda_t > 0$, while the bottom slab has the same form with $\lambda_b = -\lambda_t$. The two lattices are in registry with each other, and the surfaces are brought into proximity, with the coupling being of the same form as in Eq. (38). The formalism of Section I C is general enough to accommodate this situation with the appropriate replacements for

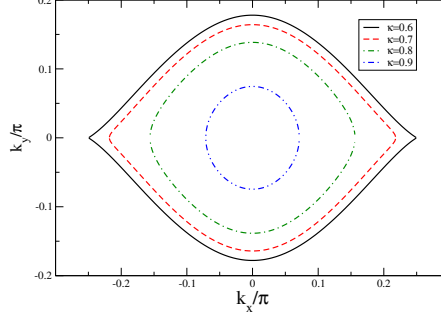


FIG. 5: Evolution of the Fermi arcs of the interface of two slabs with a tunnel-coupling κ at the surface. Both slabs have bulk Weyl points at $(\pm k_0, 0, 0)$. The values of the parameters are $k_0 = \frac{\pi}{4}$, $t' = \sin \frac{\pi}{3}$. The top slab has $\lambda = 2$ (see Eq. (45)), while the bottom slab as $\lambda = -2$. For small values of the tunnel-coupling κ , the Fermi arcs end at the projections of the Weyl points on the surface BZ. However, beyond a critical $\kappa^* \approx 0.65$ the Fermi arcs detach from the projections of the Weyl points and form an independent closed loop in the surface Brillouin zone. This loop shrinks as κ increases, and vanishes for $\kappa > 1$.

$f_y^{(t)}$, $f_y^{(b)}$, so the implicit equation for the Fermi arcs is once again given by the vanishing of the determinant of the appropriate M matrix.

In Fig. (5) we show the evolution of the Fermi arcs as the coupling strength κ between the two surfaces is increased. There is a critical value of $\kappa^* \approx 0.65$ beyond which the Fermi arcs detach from the projections of the Weyl points and form a closed loop detached from the Weyl point projections.

-
- ¹ S. Jia, S.-Y. Xu, and M. Z. Hasan, *Nature Materials* **15**, 1140 (2016), URL <https://doi.org/10.1038/nmat4787>.
 - ² N. P. Armitage, E. J. Mele, and A. Vishwanath, *Rev. Mod. Phys.* **90**, 015001 (2018), URL <https://link.aps.org/doi/10.1103/RevModPhys.90.015001>.
 - ³ C.-L. Zhang, S.-Y. Xu, I. Belopolski, Z. Yuan, Z. Lin, B. Tong, G. Bian, N. Alidoust, C.-C. Lee, S.-M. Huang, et al., *Nature Communications* **7**, 10735 (2016), article, URL <https://doi.org/10.1038/ncomms10735>.
 - ⁴ S. Murakami, *New Journal of Physics* **9**, 356 (2007), URL <https://doi.org/10.1088%2F1367-2630%2F9%2F9%2F356>.
 - ⁵ X. Wan, A. M. Turner, A. Vishwanath, and S. Y. Savrasov, *Phys. Rev. B* **83**, 205101 (2011), URL <https://link.aps.org/doi/10.1103/PhysRevB.83.205101>.
 - ⁶ K.-Y. Yang, Y.-M. Lu, and Y. Ran, *Phys. Rev. B* **84**, 075129 (2011), URL <https://link.aps.org/doi/10.1103/PhysRevB.84.075129>.
 - ⁷ G. Xu, H. Weng, Z. Wang, X. Dai, and Z. Fang, *Phys. Rev. Lett.* **107**, 186806 (2011), URL <https://link.aps.org/doi/10.1103/PhysRevLett.107.186806>.
 - ⁸ A. A. Burkov and L. Balents, *Phys. Rev. Lett.* **107**, 127205 (2011), URL <https://link.aps.org/doi/10.1103/PhysRevLett.107.127205>.
 - ⁹ T. Jungwirth, Q. Niu, and A. H. MacDonald, *Phys. Rev. Lett.* **88**, 207208 (2002), URL <https://link.aps.org/doi/10.1103/PhysRevLett.88.207208>.
 - ¹⁰ Z. Fang, N. Nagaosa, K. S. Takahashi, A. Asamitsu, R. Mathieu, T. Ogasawara, H. Yamada, M. Kawasaki, Y. Tokura, and K. Terakura, *Science* **302**, 92 (2003), ISSN 0036-8075, <https://science.sciencemag.org/content/302/5642/92.full.pdf>, URL <https://science.sciencemag.org/content/302/5642/92>.
 - ¹¹ S. A. Parameswaran, T. Grover, D. A. Abanin, D. A. Pesin, and A. Vishwanath, *Phys. Rev. X* **4**, 031035 (2014), URL <https://link.aps.org/doi/10.1103/PhysRevX.4.031035>.
 - ¹² Y. Baum, E. Berg, S. A. Parameswaran, and A. Stern, *Phys. Rev. X* **5**, 041046 (2015), URL <https://link.aps.org/doi/10.1103/PhysRevX.5.041046>.
 - ¹³ C. Zhang, E. Zhang, W. Wang, Y. Liu, Z.-G. Chen, S. Lu, S. Liang, J. Cao, X. Yuan, L. Tang, et al., *Nature Communications* **8**, 13741 EP (2017), article, URL <https://doi.org/10.1038/ncomms13741>.
 - ¹⁴ T. Ojanen, *Phys. Rev. B* **87**, 245112 (2013), URL <https://link.aps.org/doi/10.1103/PhysRevB.87.245112>.
 - ¹⁵ A. C. Potter, I. Kimchi, and A. Vishwanath, *Nature Communications* **5**, 5161 (2014), article, URL <https://doi.org/10.1038/ncomms6161>.
 - ¹⁶ P. J. W. Moll, N. L. Nair, T. Helm, A. C. Potter, I. Kimchi, A. Vishwanath, and J. G. Analytis, *Nature* **535**, 266 (2016), URL <https://doi.org/10.1038/nature18276>.
 - ¹⁷ C. Zhang, Y. Zhang, X. Yuan, S. Lu, J. Zhang, A. Narayan, Y. Liu, H. Zhang, Z. Ni, R. Liu, et al., *Nature* **565**, 331 (2019), ISSN 1476-4687, URL <https://doi.org/10.1038/s41586-018-0798-3>.
 - ¹⁸ V. Dwivedi, *Phys. Rev. B* **97**, 064201 (2018), URL <https://link.aps.org/doi/10.1103/PhysRevB.97.064201>.
 - ¹⁹ H. Ishida and A. Liebsch, *Phys. Rev. B* **98**, 195426 (2018), URL <https://link.aps.org/doi/10.1103/PhysRevB.98.195426>.

- ²⁰ K. S. Novoselov, A. Mishchenko, A. Carvalho, and A. H. Castro Neto, *Science* **353** (2016), ISSN 0036-8075, <http://science.sciencemag.org/content/353/6298/aac9439.full.pdf>, URL <http://science.sciencemag.org/content/353/6298/aac9439>.
- ²¹ D. L. Duong, S. J. Yun, and Y. H. Lee, *ACS Nano* **11**, 11803 (2017), pMID: 29219304, <https://doi.org/10.1021/acsnano.7b07436>, URL <https://doi.org/10.1021/acsnano.7b07436>.
- ²² R. Bistritzer and A. H. MacDonald, *Proceedings of the National Academy of Sciences* **108**, 12233 (2011), ISSN 0027-8424, <http://www.pnas.org/content/108/30/12233.full.pdf>, URL <http://www.pnas.org/content/108/30/12233>.
- ²³ P. San-Jose, J. González, and F. Guinea, *Phys. Rev. Lett.* **108**, 216802 (2012), URL <https://link.aps.org/doi/10.1103/PhysRevLett.108.216802>.
- ²⁴ Y. Cao, V. Fatemi, A. Demir, S. Fang, S. L. Tomarken, J. Y. Luo, J. D. Sanchez-Yamagishi, K. Watanabe, T. Taniguchi, E. Kaxiras, et al., *Nature* **556**, 80 (2018), URL <http://dx.doi.org/10.1038/nature26154>.
- ²⁵ Y. Cao, V. Fatemi, S. Fang, K. Watanabe, T. Taniguchi, E. Kaxiras, and P. Jarillo-Herrero, *Nature* **556**, 43 (2018), URL <http://dx.doi.org/10.1038/nature26160>.
- ²⁶ A. Ardavan, J. M. Schrama, S. J. Blundell, J. Singleton, W. Hayes, M. Kurmoo, P. Day, and P. Goy, *Phys. Rev. Lett.* **81**, 713 (1998), URL <https://link.aps.org/doi/10.1103/PhysRevLett.81.713>.
- ²⁷ C.-X. Liu, X.-L. Qi, H. Zhang, X. Dai, Z. Fang, and S.-C. Zhang, *Phys. Rev. B* **82**, 045122 (2010), URL <https://link.aps.org/doi/10.1103/PhysRevB.82.045122>.
- ²⁸ P. G. Silvestrov, P. W. Brouwer, and E. G. Mishchenko, *Phys. Rev. B* **86**, 075302 (2012), URL <http://link.aps.org/doi/10.1103/PhysRevB.86.075302>.
- ²⁹ L. Brey and H. A. Fertig, *Phys. Rev. B* **89**, 084305 (2014).
- ³⁰ Note that these equations do not contain Berry's curvature terms, as the Fermi arc states are spin-polarized, and the phases of $w_{d,u}$ are not expected to have significant \mathbf{k} dependence in the regions where Fermi arcs on opposite sides of the interface are degenerate.
- ³¹ C.-K. Lu and H. A. Fertig, *Phys. Rev. B* **90**, 115436 (2014), URL <https://link.aps.org/doi/10.1103/PhysRevB.90.115436>.
- ³² M. M. Vazifeh and M. Franz, *Phys. Rev. Lett.* **111**, 027201 (2013), URL <https://link.aps.org/doi/10.1103/PhysRevLett.111.027201>.
- ³³ S. Verma, D. Giri, H. A. Fertig, and A. Kundu (2019), arxiv:1908.04554.